NASA TECHNICAL MEMORANDUM

NASA TM X-2164

NASA TM X-2164

AERODYNAMIC DAMPING AND OSCILLATORY STABILITY IN PITCH AND YAW OF A VARIABLE-SWEEP SUPERSONIC TRANSPORT CONFIGURATION AT MACH NUMBERS FROM 0.40 TO 1.80

by Robert A. Kilgore

Langley Research Center
Hampton, Va. 23365

NATIONAL AERONAUTICS AND SPACE ADMINISTRATION • WASHINGTON, D. C. • FEBRUARY 1971

1. Report No.	2. Government Accession No.	3. Recipient's Catalog No.
NASA TM X-2164		

4. Title and Subtitle	5. Report Date
AERODYNAMIC DAMPING AND OSCILLATORY STABILITY IN PITCH AND YAW OF A VARIABLE-SWEEP SUPERSONIC TRANSPORT CONFIGURATION AT MACH NUMBERS FROM 0.40 TO 1.80	February 1971
	6. Performing Organization Code

7. Author(s)	8. Performing Organization Report No.
Robert A. Kilgore	L-7429
	10. Work Unit No.
	126-13-10-04

9. Performing Organization Name and Address	11. Contract or Grant No.
NASA Langley Research Center Hampton, Va. 23365	
	13. Type of Report and Period Covered
	Technical Memorandum

12. Sponsoring Agency Name and Address	14. Sponsoring Agency Code
National Aeronautics and Space Administration Washington, D.C. 20546	

15. Supplementary Notes

16. Abstract

Wind-tunnel measurements have been made with wing leading-edge sweep angles of 25° at Mach numbers of 0.40 and 0.80, 50° at Mach numbers of 0.80, 0.90, 1.00, and 1.20, and 75° at a Mach number of 1.80. The investigation was made at an oscillation amplitude of about 1° by using a forced-oscillation technique. The effects of horizontal and vertical tails, as well as the effect of horizontal-tail height, were investigated. The engine inlets were blocked since internal flow through the engines could not be simulated. In order to determine qualitatively the effect of blocking the engine inlets, tests were also made with a configuration having an ogive nose.

17. Key Words (Suggested by Author(s))	18. Distribution Statement
Variable sweep Damping in pitch Damping in yaw	Unclassified – Unlimited

19. Security Classif. (of this report)	20. Security Classif. (of this page)	21. No. of Pages	22. Price*
Unclassified	Unclassified	29	$3.00

*For sale by the National Technical Information Service, Springfield, Virginia 22151

AERODYNAMIC DAMPING AND OSCILLATORY STABILITY IN PITCH AND YAW OF A VARIABLE-SWEEP SUPERSONIC TRANSPORT CONFIGURATION AT MACH NUMBERS FROM 0.40 TO 1.80

By Robert A. Kilgore
Langley Research Center

SUMMARY

Wind-tunnel measurements of the aerodynamic damping and oscillatory stability in pitch and yaw of a model of a variable-sweep supersonic transport configuration have been made at Mach numbers from 0.40 to 1.80 by using a 1° amplitude forced-oscillation mechanism. The investigation was made with wing leading-edge sweep angles of 25° at Mach numbers of 0.40 and 0.80, 50° at Mach numbers of 0.80, 0.90, 1.00, and 1.20, and 75° at a Mach number of 1.80. The effects of horizontal and vertical tails, as well as the effect of horizontal-tail height, were determined. The engine inlets were blocked since internal flow through the engines could not be simulated. In order to determine qualitatively the effect of blocking the engine inlets, tests were also made with a configuration having an ogive nose.

The results of the investigation indicate that for the oscillation center which was used the complete airplane configurations generally have positive damping and oscillatory stability in both pitch and yaw except for a region of longitudinal instability at angles of attack greater than about 6° at subsonic speeds. The horizontal-tail and vertical-tail surfaces generally provide most of the damping in pitch and damping in yaw, respectively. The low horizontal tail generally provides slightly greater damping and stability in pitch than the high horizontal tail, and the increase varies with wing sweep angle and angle of attack. The levels and trends of damping and stability in pitch are generally independent of fuselage shape. The effect of fuselage shape on the lateral dynamic stability characteristics is insignificant near an angle of attack of 0° and is appreciable at angles of attack greater than about 4° to 6°.

INTRODUCTION

One of the requirements for a commercially successful supersonic transport is that the airplane have acceptable stability and control characteristics in all phases of flight. The National Aeronautics and Space Administration, therefore, has investigated the

aerodynamic characteristics of a number of proposed supersonic transport configurations, some of which employ variable-sweep wings. Some of the longitudinal and lateral dynamic stability characteristics for one of the variable-sweep supersonic transport configurations are presented in reference 1 for the configuration with wings swept back 75° for Mach numbers of 2.40, 2.98, and 3.60.

This paper presents some experimentally determined longitudinal and lateral dynamic stability characteristics at Mach numbers from 0.40 to 1.80 for the model used in the investigation of reference 1. The model was tested with wing leading-edge sweep angles of 25° at Mach numbers of 0.40 and 0.80, 50° at Mach numbers of 0.80, 0.90, 1.00, and 1.20, and 75° at a Mach number of 1.80. The tests were made at an oscillation amplitude of about 1° by using a forced-oscillation technique.

Tests were made to determine the effect of removal of the horizontal and vertical tails and of changing the horizontal-tail height. The model was tested with the engine inlets blocked since the space required for the oscillation-balance mechanism prevented internal flow through the engine ducts. Since it was recognized that blocked engine inlets would not provide a correct simulation of flow over the model, tests also were made with the model equipped with an ogive nose faired into the fuselage in order to provide a qualitative comparison of the effects of blocked engine inlets on the dynamic stability characteristics.

SYMBOLS

Measurements and calculations were made in the U.S. Customary Units; however, they are presented in this text in the International System of Units (SI). Details concerning the use of SI, together with physical constants and conversion factors, are given in reference 2.

The aerodynamic parameters are referred to the body system of axes as shown in figure 1. These axes originate at the oscillation center of the model, as shown in the detail drawings which are presented in figure 2. The equations which were used to reduce the dimensional aerodynamic parameters of the models to the nondimensional aerodynamic parameters are presented in the section entitled "Measurements and Reduction of Data." The reference dimensions are based on the geometric characteristics of the model with the wings in the 75° sweep position, regardless of the actual test wing-sweep position.

b reference span, 0.491 meter

$\bar{c}$ reference chord (mean geometric chord), 0.357 meter

f	frequency of oscillation, hertz
k	reduced-frequency parameter, $\frac{\omega\bar{c}}{2V}$ in pitch, $\frac{\omega b}{2V}$ in yaw, radians
M	free-stream Mach number
q	angular velocity of body-axis system about Y-axis, radians/second (see fig. 1)
q_∞	free-stream dynamic pressure, newtons/meter^2
R	Reynolds number based on $\bar{c}$
r	angular velocity of body-axis system about Z-axis, radians/second (see fig. 1)
S	reference area, 0.154 meter^2
V	free-stream velocity, meters/second
α	angle of attack, degrees or radians; or mean angle of attack, degrees (see fig. 1)
β	angle of sideslip, radians (see fig. 1)
Λ	angle of wing sweep, degrees
ω	angular velocity, $2\pi f$, radians/second
C_l	rolling-moment coefficient, $\frac{\text{Rolling moment}}{q_\infty Sb}$ (see fig. 1)
C_m	pitching-moment coefficient, $\frac{\text{Pitching moment}}{q_\infty S\bar{c}}$ (see fig. 1)
C_n	yawing-moment coefficient, $\frac{\text{Yawing moment}}{q_\infty Sb}$ (see fig. 1)

$C_{l_{\dot{r}}} = \frac{\partial C_l}{\partial\left(\frac{\dot{r}b^2}{4V^2}\right)}$ per radian

$C_{l_\beta} = \frac{\partial C_l}{\partial \beta}$ per radian

$$C_{m_q} = \frac{\partial C_m}{\partial\left(\frac{q\bar{c}}{2V}\right)} \text{ per radian}$$

$$C_{m_{\dot{q}}} = \frac{\partial C_m}{\partial\left(\frac{\dot{q}\bar{c}^2}{4V^2}\right)} \text{ per radian}$$

$$C_{m_\alpha} = \frac{\partial C_m}{\partial \alpha} \text{ per radian}$$

$$C_{m_{\dot{\alpha}}} = \frac{\partial C_m}{\partial\left(\frac{\dot{\alpha}\bar{c}}{2V}\right)} \text{ per radian}$$

$$C_{n_r} = \frac{\partial C_n}{\partial\left(\frac{rb}{2V}\right)} \text{ per radian}$$

$$C_{n_{\dot{r}}} = \frac{\partial C_n}{\partial\left(\frac{\dot{r}b^2}{4V^2}\right)} \text{ per radian}$$

$$C_{n_\beta} = \frac{\partial C_n}{\partial \beta} \text{ per radian}$$

$$C_{n_{\dot{\beta}}} = \frac{\partial C_n}{\partial\left(\frac{\dot{\beta}b}{2V}\right)} \text{ per radian}$$

$C_{l_\beta} \cos \alpha + k^2 C_{l_{\dot{r}}}$	effective-dihedral parameter, per radian
$C_{m_q} + C_{m_{\dot{\alpha}}}$	damping-in-pitch parameter, per radian
$C_{m_\alpha} - k^2 C_{m_{\dot{q}}}$	oscillatory-longitudinal-stability parameter, per radian
$C_{n_r} - C_{n_{\dot{\beta}}} \cos \alpha$	damping-in-yaw parameter, per radian
$C_{n_\beta} \cos \alpha + k^2 C_{n_{\dot{r}}}$	oscillatory-directional-stability parameter, per radian

A dot over a quantity indicates a first derivative with respect to time. The expression $\cos \alpha$ appears in the lateral parameters since these parameters are referred to the body system of axes.

Configuration Nomenclature

The designation used herein for the various model components is as follows:

F_O	fuselage with ogive nose
F_1	fuselage with blocked-engine-inlet nose
H_1	low horizontal tail
H_2	high horizontal tail
W_{25}	wing with leading-edge sweep of 25^o
W_{50}	wing with leading-edge sweep of 50^o
W_{75}	wing with leading-edge sweep of 75^o
V	vertical tail

MODELS AND APPARATUS

Models

The models of the two basic configurations which were tested are shown in the air-brush drawings of figure 2 and photographs of figure 3. As previously mentioned, the model used in this investigation is the same model as was used in reference 1.

The model was made of magnesium, aluminum, and plastic-impregnated fiber glass. The wings are adjustable so that leading-edge sweep angles of 25^o, 50^o, and 75^o can be obtained. The wings in the 25^o sweep position have NACA 65A006 thickness distributions parallel to the airstream and are cambered to provide flat undersurfaces. A wing twist of 2^o washout is developed about the 50-percent-chord line. The horizontal and vertical tails have 3-percent-thickness distributions parallel to the airstream and are based on NACA 65-series airfoil sections. Provisions were made for changing the height of the horizontal tail and for removing both the horizontal and vertical tails. A detail drawing of the wing and horizontal tail is presented in figure 4.

Two interchangeable nose sections were provided for the fuselage. The nose section shown in figure 2(a) has a simulated engine inlet with blocked air passages. The other nose section, shown in figure 2(b), has a tangent ogive which is faired into the

fuselage near the wing root. As previously mentioned, no provision was made for flow through the engines because of the space required for the oscillation-balance mechanism.

The reference dimensions used to reduce the data are based on the geometric characteristics of the model with the wings in the 75° sweep position, regardless of the actual test wing-sweep position. Actual model geometric characteristics are as follows:

Wing sweep angle, Λ, deg	Span, b, m	Mean geometric chord, $\bar{c}$, m	Wing area, S, m^2
25	0.972	0.140	0.188
50	.799	.235	.158
75	.491	.357	.154

Three-dimensional roughness in the form of 0.0025-meter-wide bands of sparsely distributed No. 60 carborundum grains was applied to the wing and tail surfaces at the 10-percent-streamwise-chord line (defined for the wing in the 50° sweep position). The roughness size and location were not changed when the wing sweep was changed to 25° or to 75°. A similar band of roughness was applied around the fuselage approximately 0.051 meter from the nose.

Apparatus

Oscillation mechanism.- Exploded and assembled views of the forward portion of the oscillation-balance mechanism which was used for these tests are presented in figure ure 5. Since the amplitude of the forced oscillation was small (1°), the rotary motion of an electric motor was used to provide essentially sinusoidal motion of constant amplitude to the balance through the crank and Scotch yoke mechanism. The oscillatory motion was about the pivot axis, which was located at the proposed center-of-mass location of the configuration.

The strain-gage bridge used to measure the torque required to oscillate the model was located between the model mounting surface and the pivot axis. This bridge location eliminated the pivot friction characteristics from the model system and thereby eliminated the need to correct the data for varying pivot friction associated with changing aerodynamic load. Although the torque bridge was physically forward of the pivot axis, all torques were measured with respect to the pivot axis.

The mechanical spring shown in the photograph (fig. 5) was installed between the model mounting surface and the fixed sting. The strain-gage bridge which was attached to the mechanical spring was used to determine the amplitude of the model angular displacement with respect to the fixed sting. The mechanical spring allowed the model system to be oscillated at velocity resonance.

For the yawing tests, a rolling-torque balance was attached to the front of the oscillation balance to provide measurements of the rolling torque induced by the yawing motion.

Wind tunnels.- Two wind tunnels were used to obtain the data presented herein. Common to both tunnels is the ability to control relative humidity and total temperature of the air in the tunnel in order to minimize the effects of condensation shocks and the ability to control total pressure in order to obtain the desired Reynolds number.

The data for Mach numbers from 0.40 to 1.20 were obtained in the Langley 8-foot transonic pressure tunnel. The test section of this single-return wind tunnel is about 2.2 meters square with slotted upper and lower walls to permit continuous operation through the transonic speed range. Test-section Mach numbers from near 0 to 1.30 can be obtained and kept constant by controlling the speed of the tunnel-fan drive motor. The sting support strut is so designed as to keep the model near the center line of the tunnel through a range of angle of attack from about -5° to 16° when used in conjunction with the oscillation-balance mechanism that was used for these tests.

The data for a Mach number of 1.80 were obtained in test section number 1 of the Langley Unitary Plan wind tunnel. This single-return tunnel has a test section about 1.2 meters square and about 2.1 meters long. An asymmetric sliding block is used to vary the area ratio in order to change the Mach number from about 1.47 to 2.87. The angle-of-attack mechanism that was used for these tests has a total range of about 25° when used in conjunction with the oscillation-balance mechanism. A photograph of one of the models installed on the oscillation-balance mechanism in the wind-tunnel test section is presented as figure 6. A more complete description of the Langley 8-foot transonic pressure tunnel and the Langley Unitary Plan wind tunnel is given in reference 3.

MEASUREMENTS AND REDUCTION OF DATA

The strain-gage bridges used to measure the torque required to oscillate the model, the rolling torque (for yawing tests only), and the angular displacement of the model with respect to the sting are powered by 3000-hertz carrier voltage. The bridge outputs are proportional to the instantaneous torque and the instantaneous angular displacement. The constant components of the bridge outputs are removed by using conventional bridge-balance circuits. The nonconstant components are amplified and passed through mechanically coupled but electrically independent sine-cosine resolvers which rotate with constant angular velocity at the frequency of model oscillation and resolve each signal into two components. The components are rectified by phase-sensitive demodulators and read-on damped digital voltmeters to provide direct-current voltage proportional to the orthogonal components of the amplitude of the torque required to oscillate the model, the rolling torque, and the angular displacement of the model with respect to the sting. The

amplitudes of torque, rolling torque, and displacement are then computed from their respective orthogonal components. The individual resolvers are electrically alined so that the phase angle between the torque required to oscillate the model and angular displacement and between the rolling torque and angular displacement may also be determined from the orthogonal components.

The resolver-damped—voltmeter system acts as an extremely narrow band-pass filter with the center frequency always being the frequency of oscillation of the model. In this way, as explained in reference 4, the effects of random torque inputs due to tunnel turbulence or other causes are eliminated and only the components of torque and angular displacement which occur at the frequency of oscillation are used in computing the dynamic stability characteristics of the model.

The frequency of oscillation was measured by using an electronic counter to count for 1 second the pulses generated by an induction-coil pickup and a 100-tooth gear which was fastened to the shaft of one of the resolvers.

For the pitching tests, measurements were made of the amplitude of the torque required to oscillate the model in pitch T_Y, the amplitude of the angular displacement in pitch of the model with respect to the sting Θ, the phase angle η between T_Y and Θ, and the angular velocity of the forced oscillation ω. The viscous-damping coefficient in pitch for this single-degree-of-freedom system was computed as

$$C_Y = \frac{T_Y \sin \eta}{\omega \Theta} \tag{1}$$

and the spring-inertia parameter in pitch was computed as

$$K_Y - I_Y \omega^2 = \frac{T_Y \cos \eta}{\Theta} \tag{2}$$

where K_Y is the torsional-spring coefficient of the system and I_Y is the moment of inertia of the system about the body Y-axis.

For these tests, the damping-in-pitch parameter was computed as

$$C_{m_q} + C_{m_{\dot{\alpha}}} = -\frac{2V}{q_\infty S \bar{c}^2}\left[(C_Y)_{\text{wind on}} - (C_Y)_{\text{wind off}}\right] \tag{3}$$

and the oscillatory-longitudinal-stability parameter was computed as

$$C_{m_\alpha} - k^2 C_{m_{\dot{q}}} = -\frac{1}{q_\infty S \bar{c}}\left[(K_Y - I_Y \omega^2)_{\text{wind on}} - (K_Y - I_Y \omega^2)_{\text{wind off}}\right] \tag{4}$$

The wind-off value of C_Y is determined at the frequency of wind-off velocity resonance since the value of C_Y is independent of frequency and can be determined most accurately

at the frequency of velocity resonance. The wind-on and wind-off values of $K_Y - I_Y\omega^2$ are determined at the same frequency since $K_Y - I_Y\omega^2$ is a function of frequency.

For the yawing tests, measurements were made of the amplitude of the torque required to oscillate the model in yaw T_Z, the amplitude of the angular displacement in yaw of the model with respect to the sting Ψ, the phase angle λ between T_Z and Ψ, and the angular velocity of the forced oscillation ω.

The system characteristics in yaw, referred to the body Z-axis, were computed as

$$C_Z = \frac{T_Z \sin \lambda}{\omega \Psi} \tag{5}$$

and

$$K_Z - I_Z\omega^2 = \frac{T_Z \cos \lambda}{\Psi} \tag{6}$$

where K_Z is the torsional-spring coefficient of the system and I_Z is the moment of inertia of the system about the body Z-axis.

For these tests, the damping-in-yaw parameter was computed as

$$C_{n_r} - C_{n_{\dot{\beta}}} \cos \alpha = -\frac{2V}{q_\infty Sb^2}\left[(C_Z)_{\text{wind on}} - (C_Z)_{\text{wind off}}\right] \tag{7}$$

and the oscillatory-directional-stability parameter was computed as

$$C_{n_\beta} \cos \alpha + k^2 C_{n_{\dot{r}}} = \frac{1}{q_\infty Sb}\left[\left(\frac{T_Z \cos \lambda}{\Psi}\right)_{\text{wind on}} - \left(\frac{T_Z \cos \lambda}{\Psi}\right)_{\text{wind off}}\right] \tag{8}$$

As for the pitching-oscillation tests, the wind-off value of C_Z is determined at the frequency of wind-off velocity resonance, and the wind-off and wind-on values of $K_Z - I_Z\omega^2$ are determined at the same frequency.

During the yawing-oscillation tests, measurements were also made of the maximum rolling torque T_X induced by the yawing oscillation and of the phase angle γ between T_X and the yawing displacement. That portion of the rolling torque in phase with yawing displacement was used to compute the following expression for the effective-dihedral parameter:

$$C_{l_\beta} \cos \alpha + k^2 C_{l_{\dot{r}}} = \frac{1}{q_\infty Sb}\left[\left(\frac{T_X \cos \gamma}{\Psi}\right)_{\text{wind on}} - \left(\frac{T_X \cos \gamma}{\Psi}\right)_{\text{wind off}}\right] \tag{9}$$

The wind-off and wind-on values of $\frac{T_X \cos \gamma}{\Psi}$ were determined at the same oscillation frequency.

Instrumentation difficulties precluded accurate measurement of that portion of the rolling torque in phase with yawing velocity. Therefore, values of $C_{l_r} - C_{l_{\dot{\beta}}} \cos \alpha$ were not computed for these tests.

TESTS

The dynamic-stability parameters in pitch were measured through a range of mean angle of attack at 0° angle of sideslip with the model oscillating in pitch about the body Y-axis. The oscillation balance was rolled 90° within the model to provide model oscillations in yaw about the body Z-axis as the dynamic-stability parameters in yaw were measured through a range of angle of attack at 0° mean angle of sideslip. The tests were made at Mach numbers from 0.40 to 1.80 at an amplitude of about 1° by using a small-amplitude forced-oscillation mechanism. Reynolds number, based on the mean geometric chord of the wing in the 75° sweep position, stagnation pressure, and stagnation temperature for the various Mach numbers were as follows:

Mach number, M	Stagnation pressure, kN/m^2	Stagnation temperature, K	Reynolds number, R
0.40	25.6	323	0.67×10^6
.80	↓	↓	1.10
.90			1.16
1.00			1.20
1.20			1.22
1.80	27.6	339	1.17

The angle of attack was varied from about 0° to about 10°. The reduced-frequency parameter was varied from 0.0135 to 0.0465 in pitch and from 0.0135 to 0.0589 in yaw. Tests were made with wing leading-edge sweep angles of 25° at Mach numbers of 0.40 and 0.80, 50° at Mach numbers of 0.80, 0.90, 1.00, and 1.20, and 75° at a Mach number of 1.80. The effects of horizontal and vertical tails, as well as the effect of horizontal-tail height, were investigated. The engine inlets were blocked since internal flow through the engines could not be simulated. Tests also were made with an ogive nose in order to determine qualitatively the effect of blocking the engine inlets.

As previously mentioned, a turbulent boundary layer over the model was assured by the use of three-dimensional roughness bands.

PRESENTATION OF RESULTS

An index to the data figures is as follows:

Wing sweep angle, Λ, deg	Mach number, M	Longitudinal stability results	Lateral stability results
25	0.40 and 0.80	Figure 7	Figure 10
50	0.80, 0.90, 1.00, and 1.20	Figure 8	Figure 11
75	1.80	Figure 9	Figure 12

Schlieren photographs taken in the plane of symmetry at $M = 1.80$ are presented as figure 13.

DISCUSSION OF RESULTS

Longitudinal Stability

$\Lambda = 25^{\circ}$, $M = 0.40$ and 0.80 (fig. 7).- Figure 7 presents the longitudinal dynamic stability of several configurations with a wing sweep angle of 25° at Mach numbers of 0.40 and 0.80. All configurations have positive damping in pitch (negative values of $C_{m_q} + C_{m_{\dot{\alpha}}}$) at all values of mean angle of attack α. Longitudinal stability generally decreases with increasing α (positive longitudinal stability is indicated by a negative value of $C_{m_\alpha} - k^2 C_{m_{\dot{q}}}$). Tests made with the horizontal tail removed (configuration $F_0W_{25}V$) show that about one-half of the damping in pitch is provided by the horizontal tail. The configuration with the low horizontal tail H_1 has slightly greater damping at all values of α than the configuration with the high horizontal tail H_2. The configuration with the low horizontal tail is slightly more stable than the configuration with the high horizontal tail at positive values of α and less stable at negative values of α. The configuration with the ogive fuselage F_O generally has greater damping than the blocked-engine-inlet fuselage F_1. Differences in stability for the two configurations are minor.

$\Lambda = 50^{\circ}$, $M = 0.80$ to 1.20 (fig. 8).- The configurations with the wing swept 50° at Mach numbers from 0.80 to 1.20 generally have positive damping in pitch except at a Mach number of 1.00. (See fig. 8.) Longitudinal stability generally decreases with increasing α. A pronounced decrease in stability occurs for all configurations near $\alpha = 6^{\circ}$ at Mach numbers of 0.80 and 0.90. Tests made with the horizontal tail removed (configuration $F_OW_{50}V$) show that a large part of the total damping in pitch is contributed by the horizontal tail. The configuration with the low horizontal tail H_1 generally has less damping at all values of α than the configuration with the high horizontal tail H_2.

This is opposite to the effect of tail height observed at $M = 0.40$ and 0.80 for the configuration with a wing sweep angle of 25° (fig. 7). The configuration with the low horizontal tail is generally more stable than the configuration with the high horizontal tail. No significant effects of fuselage shape occur for a wing sweep angle of 50°.

$\Lambda = 75^\circ$, $M = 1.80$ (fig. 9).- Figure 9 presents the longitudinal dynamic stability characteristics of several configurations with a wing sweep angle of 75° at a Mach number of 1.80. All configurations have positive damping and stability in pitch. The addition of either the low horizontal tail H_1 or the high horizontal tail H_2 generally causes an increase in damping and stability in pitch. These results are in agreement with those of reference 1 for these same configurations at Mach numbers of 2.40, 2.98, and 3.60. Although the schlieren photographs of figure 13 show detailed differences in the shock patterns produced by the ogive nose and the blocked-engine-inlet nose, the measured longitudinal stability parameters for the two configurations are very similar. Since the origin of the strong shocks from the blocked-engine-inlet nose is relatively close to the oscillation center and the shocks do not impinge on the model at $M = 1.80$, the similarity of the data might be expected.

Lateral Stability

$\Lambda = 25^\circ$, $M = 0.40$ and 0.80 (fig. 10).- Figure 10 presents the lateral dynamic stability characteristics of several configurations with a wing sweep angle of 25° at Mach numbers of 0.40 and 0.80. All configurations have positive damping in yaw (negative values of $C_{n_r} - C_{n_{\dot\beta}} \cos\alpha$) at all values of angle of attack α. Most of the damping in yaw is contributed by the vertical tail, especially at the lower values of α. Large stabilizing increments of the parameter $C_{n_\beta} \cos\alpha + k^2 C_{n_{\dot r}}$ are contributed by the vertical tail. All configurations generally exhibit positive effective dihedral (a negative value of $C_{l_\beta} \cos\alpha + k^2 C_{l_{\dot r}}$), with the vertical tail adding an almost constant positive dihedral effect through the α range. The damping in yaw is generally independent of fuselage shape. However, the directional stability and effective dihedral parameters are affected by fuselage shape, especially at angles of attack above about 8°.

$\Lambda = 50^\circ$, $M = 0.80$ to 1.20 (fig. 11).- Figure 11 presents the lateral dynamic stability characteristics of three configurations with a wing sweep angle of 50° at Mach numbers from 0.80 to 1.20. All configurations have positive damping in yaw, with a pronounced increase in damping occurring at the higher angles of attack. At the lower values of α, the vertical tail is the main contributor to both damping and stability in yaw. The levels and trends of damping are independent of fuselage shape up to angles of attack of about 4°. At the higher angles of attack, the configuration with the ogive nose F_O has more damping and less stability than the configuration with the blocked-engine-inlet nose

F_1. All configurations exhibit positive effective dihedral except the configuration without the vertical tail $(F_O W_{50} H_1)$ near $\alpha = 0^O$ at $M = 1.00$ and 1.20.

$\Lambda = 75^O$, $M = 1.80$ (fig. 12).- Figure 12 presents the lateral dynamic stability characteristics of two configurations with a wing sweep angle of 75^O at a Mach number of 1.80. The addition of the vertical tail V increases the damping and stability in yaw and adds a negative increment to the effective dihedral parameter at all angles of attack. These results are in agreement with those of reference 1 for these same configurations at Mach numbers of 2.40, 2.98, and 3.60.

CONCLUDING REMARKS

Wind-tunnel measurements of the aerodynamic damping and oscillatory stability in pitch and yaw of a model of a variable-sweep supersonic transport configuration have been made at Mach numbers from 0.40 to 1.80 by using a 1^O amplitude forced-oscillation mechanism. The investigation was made with wing leading-edge sweep angles of 25^O at Mach numbers of 0.40 and 0.80, 50^O at Mach numbers of 0.80, 0.90, 1.00, and 1.20, and 75^O at a Mach number of 1.80. The effects of horizontal and vertical tails, as well as the effect of horizontal-tail height, were detemined. The engine inlets were blocked since internal flow through the engines could not be simulated. In order to determine qualitatively the effect of blocking the engine inlets, tests were also made with a configuration having an ogive nose.

The results of the investigation indicate that for the oscillation center which was used the complete airplane configurations generally have positive damping and oscillatory stability in both pitch and yaw except for a region of longitudinal instability at angles of attack greater than about 6^O at subsonic speeds. The horizontal-tail and vertical-tail surfaces generally provide most of the damping in pitch and damping in yaw, respectively. The low horizontal tail generally provides slightly greater damping and stability in pitch than the high horizontal tail, and the increase varies with wing sweep angle and angle of attack. The levels and trends of damping and stability in pitch are generally independent of fuselage shape. The effect of fuselage shape on the lateral dynamic stability characteristics is insignificant near an angle of attack of 0^O and is appreciable at angles of attack greater than about 4^O to 6^O.

Langley Research Center,
National Aeronautics and Space Administration,
Hampton, Va., December 23, 1970.

REFERENCES

1. Delaney, Bobby R.; and Thompson, Wilson E.: Dynamic Stability Characteristics in Pitch and in Yaw for a Model of a Variable-Sweep Supersonic Transport Configuration at Mach Numbers of 2.40, 2.98, and 3.60. NASA TM X-761, 1963.

2. Mechtly, E. A.: The International System of Units – Physical Constants and Conversion Factors (Revised). NASA SP-7012, 1969.

3. Schaefer, William T., Jr.: Characteristics of Major Active Wind Tunnels at the Langley Research Center. NASA TM X-1130, 1965.

4. Braslow, Albert L.; Wiley, Harleth G.; and Lee, Cullen Q.: A Rigidly Forced Oscillation System for Measuring Dynamic-Stability Parameters in Transonic and Supersonic Wind Tunnels. NASA TN D-1231, 1962.

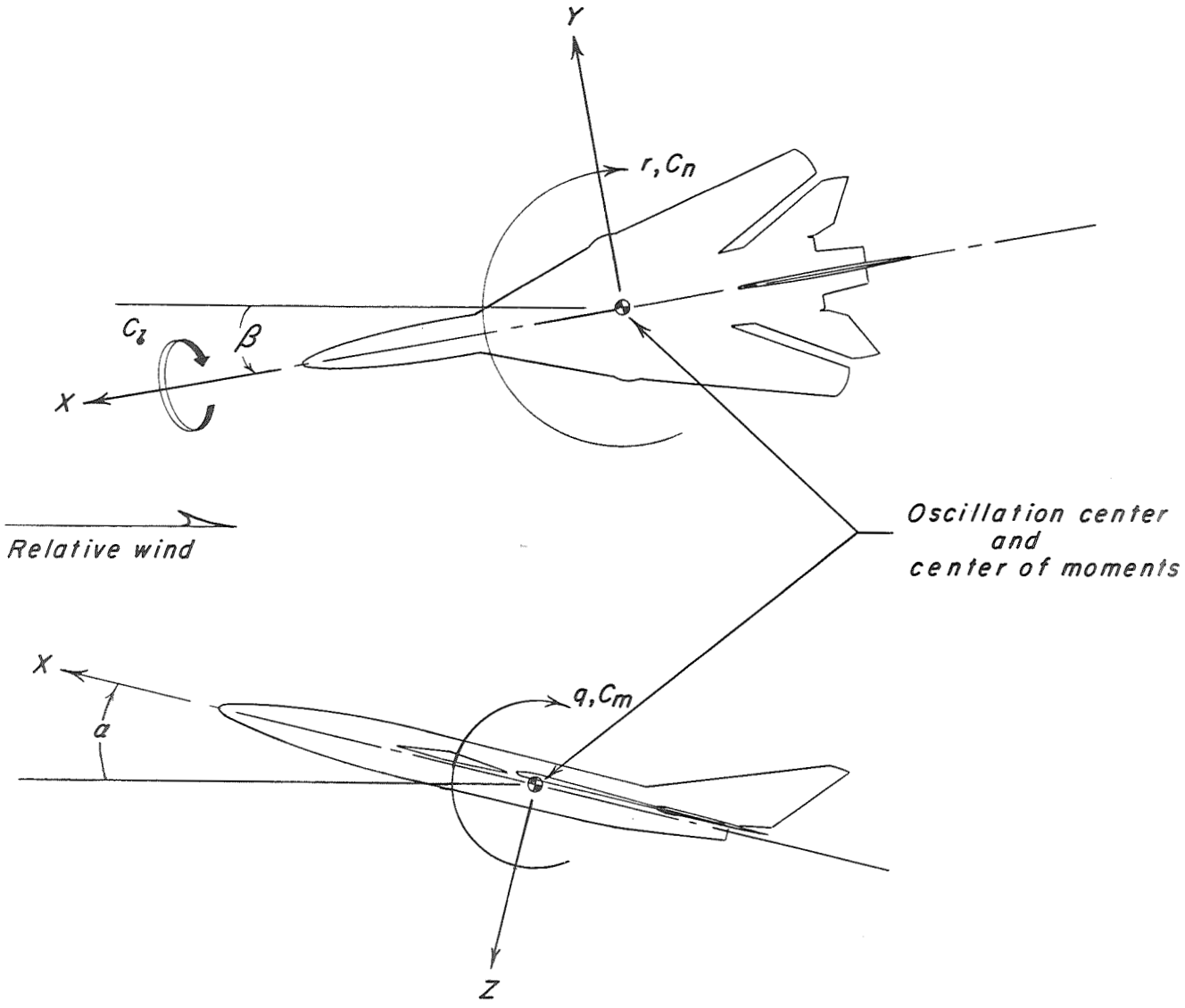

Figure 1.- Body system of axes. All angles, angular velocities, and coefficients shown in positive sense.

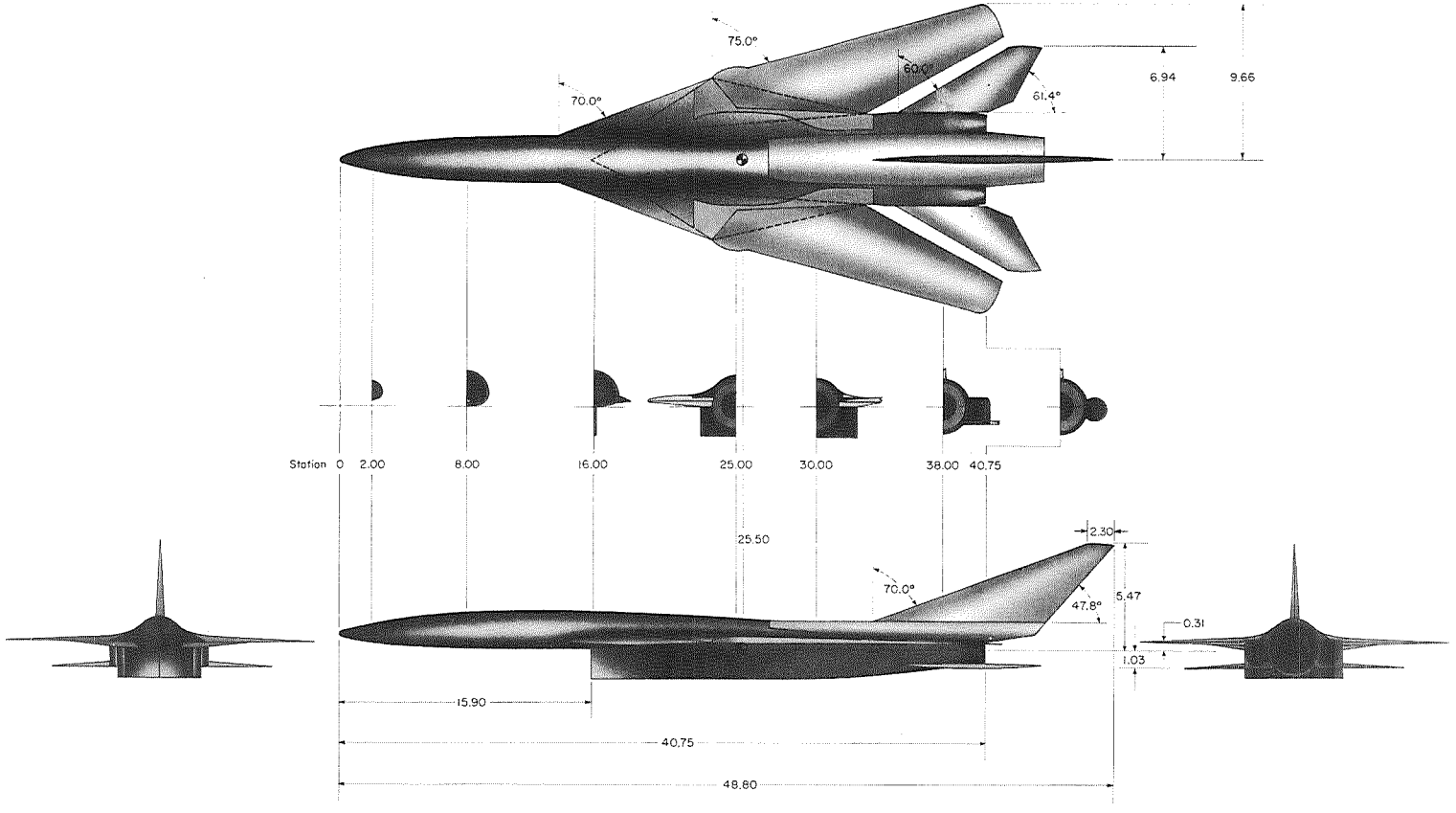

(a) Configuration with blocked-engine-inlet nose and low horizontal tail $\left(F_1W_{75}VH_1\right)$.

Figure 2.- Detail drawings of models. All linear dimensions in inches (1 inch = 0.0254 meter).

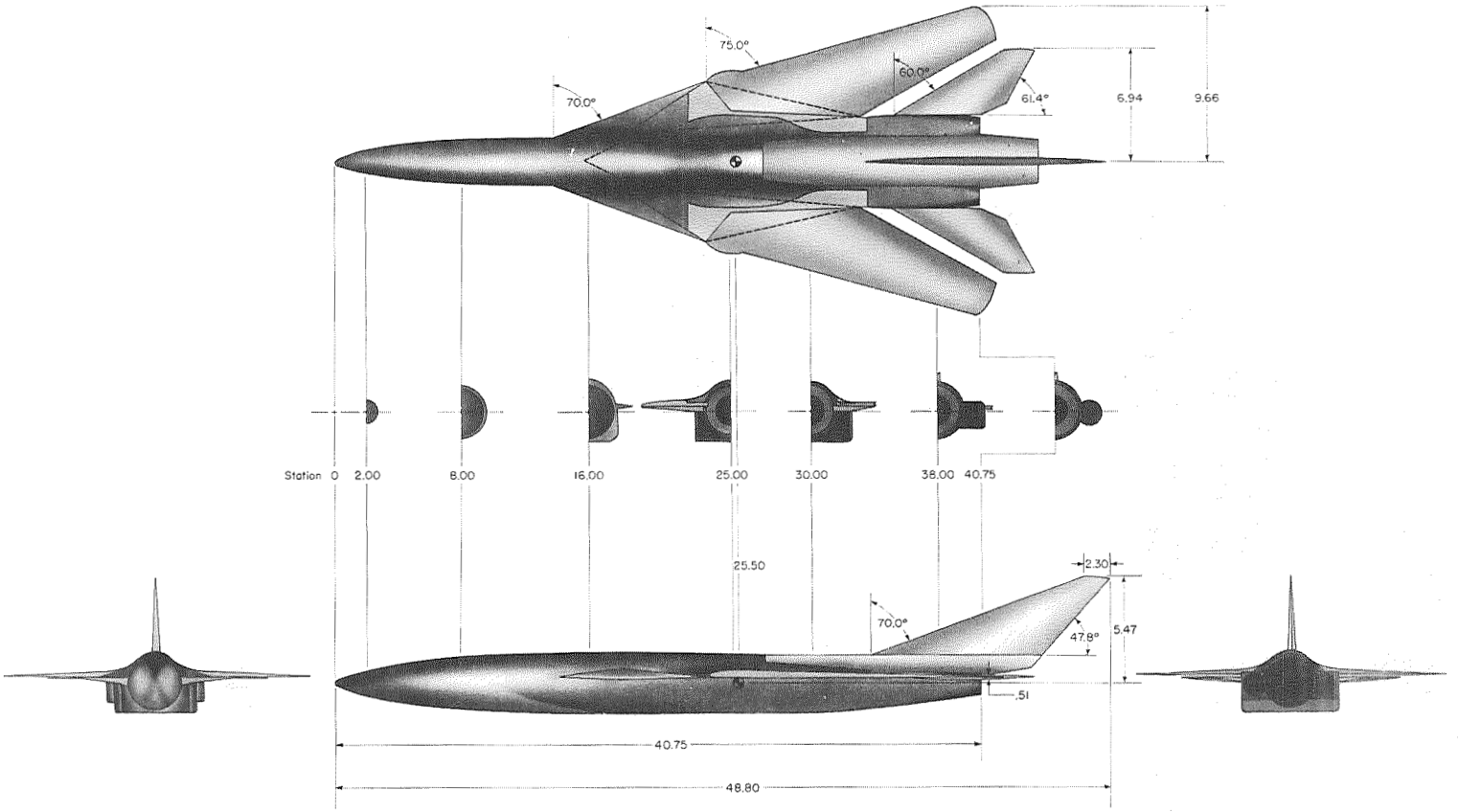

(b) Configuration with ogive nose and high horizontal tail $(F_O W_{75} V H_2)$.

Figure 2.- Concluded.

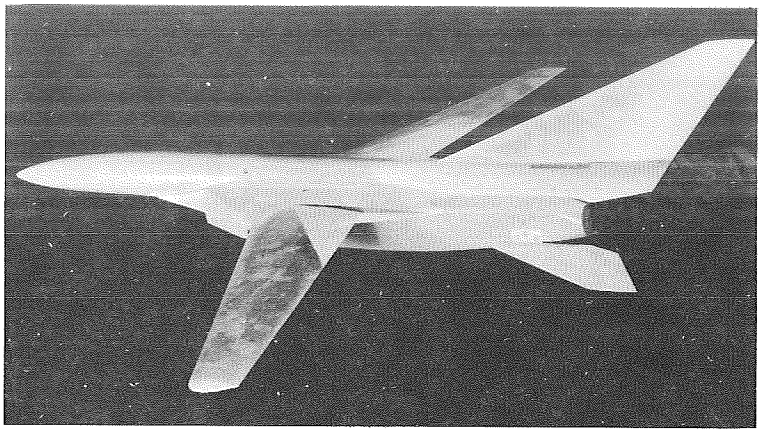

$F_1 W_{25} VH_1$

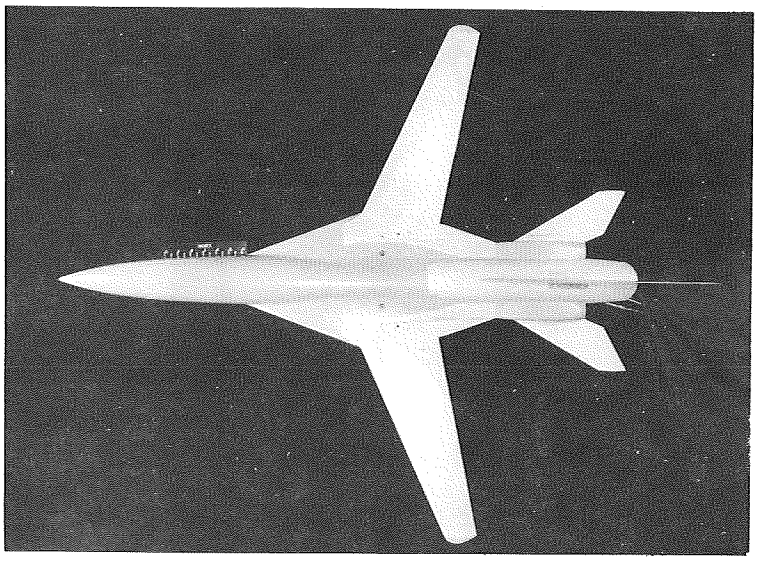

$F_0 W_{25} VH_1$

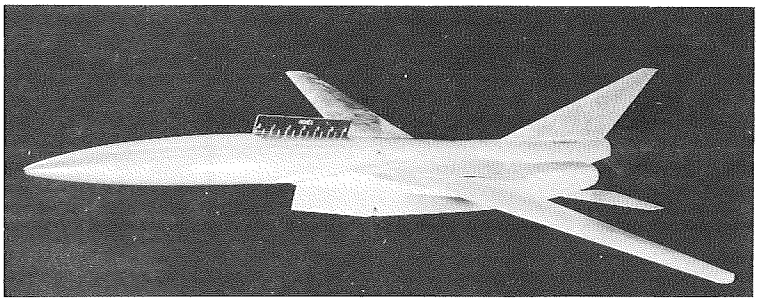

$F_1 W_{25} VH_1$

L-70-8034

(a) Wing sweep angle of 25^{o}.

Figure 3.- Photographs of models.

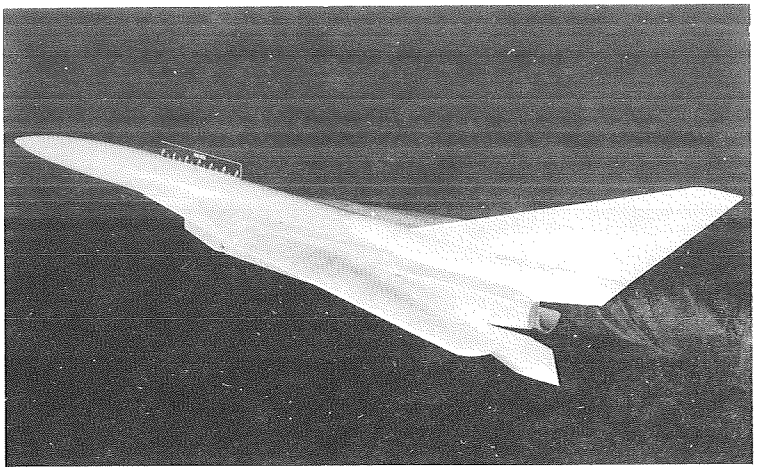

$F_1 W_{75} VH_1$

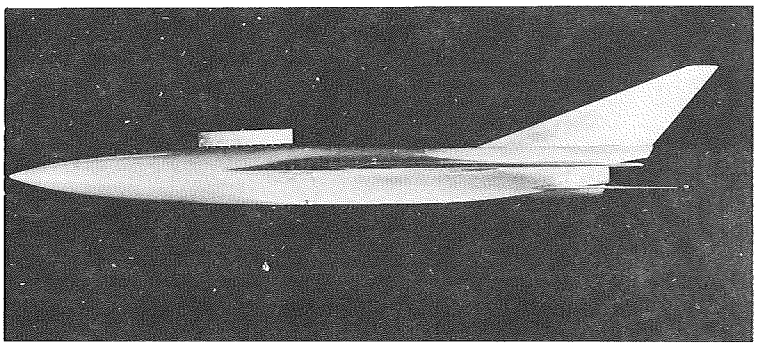

$F_0 W_{75} VH_1$

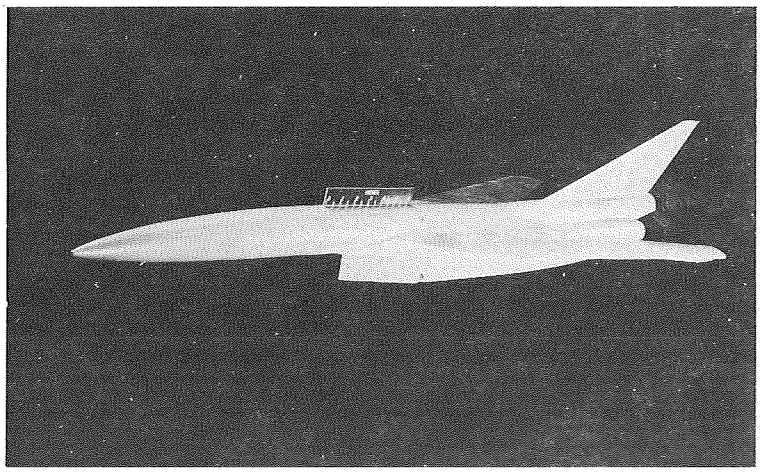

$F_1 W_{75} VH_1$

L-70-8035

(b) Wing sweep angle of 75°.

Figure 3.- Concluded.

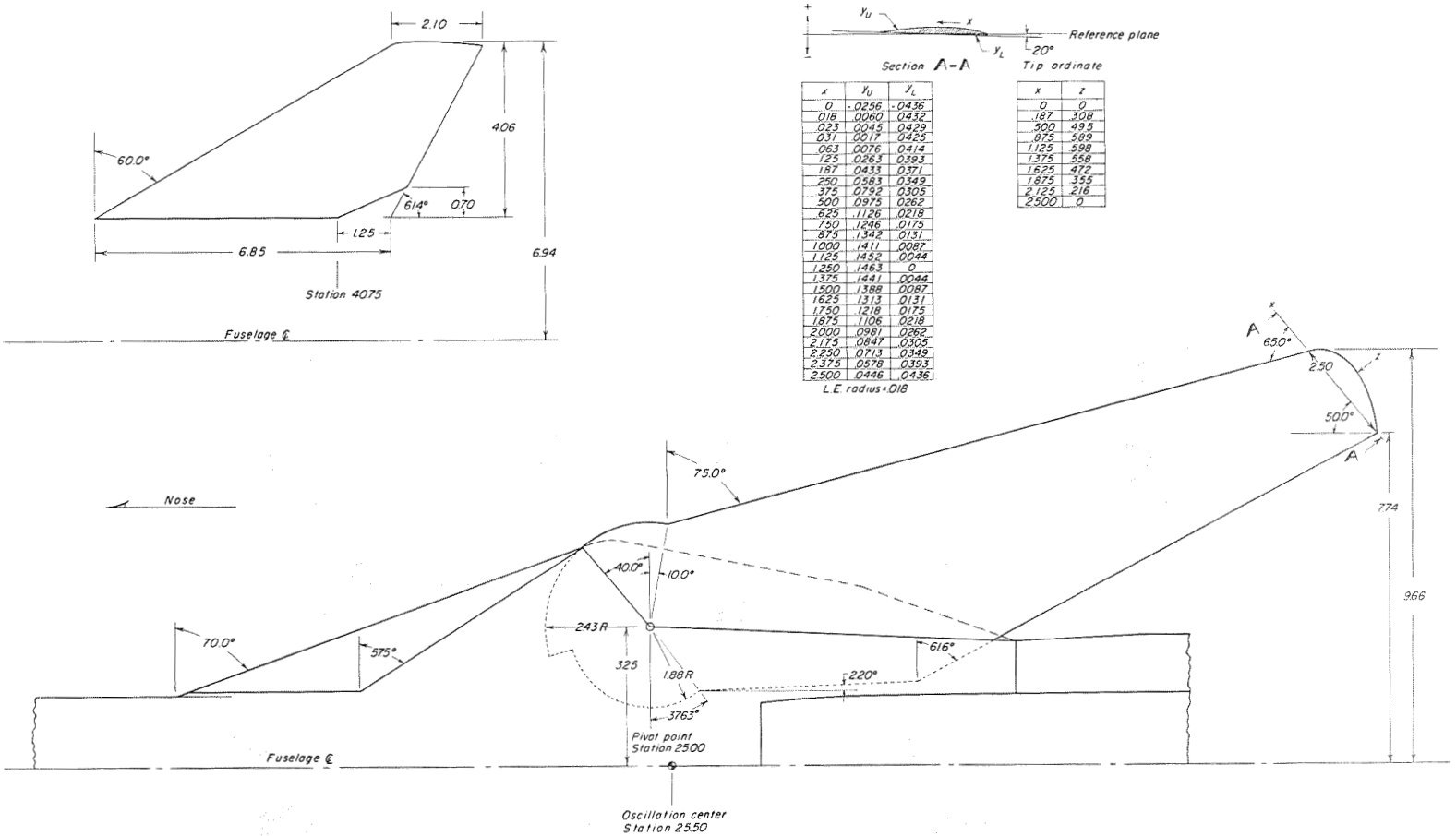

x	y_U	y_L
0	.0256	.0436
.018	.0060	.0432
.023	.0045	.0429
.031	.0017	.0425
.063	.0076	.0414
.125	.0263	.0393
.187	.0433	.0371
.250	.0583	.0349
.375	.0792	.0305
.500	.0975	.0262
.625	.1126	.0218
.750	.1246	.0175
.875	.1342	.0131
1.000	.1411	.0087
1.125	.1452	.0044
1.250	.1463	0
1.375	.1441	.0044
1.500	.1388	.0087
1.625	.1313	.0131
1.750	.1218	.0175
1.875	.1106	.0218
2.000	.0981	.0262
2.175	.0847	.0305
2.250	.0713	.0349
2.375	.0578	.0393
2.500	.0446	.0436

x	z
0	0
.187	.308
.500	.495
.875	.589
1.125	.598
1.375	.558
1.625	.472
1.875	.355
2.125	.216
2.500	0

Figure 4.- Details of wing and horizontal tail. All linear dimensions in inches (1 inch = 0.0254 meter).

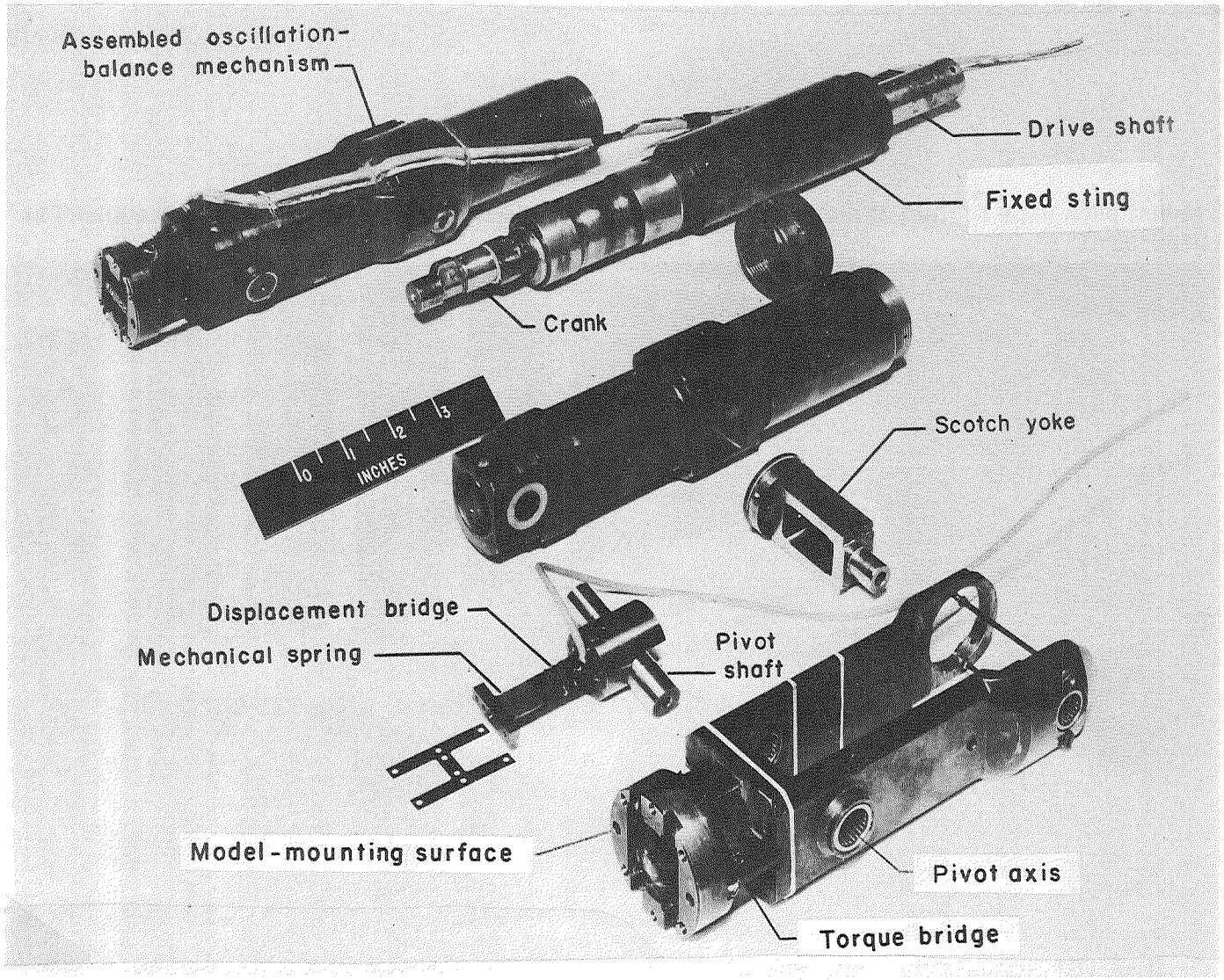

L-63-1969.3

Figure 5.- Forward portion of oscillation-balance mechanism. (1 inch = 0.0254 meter).

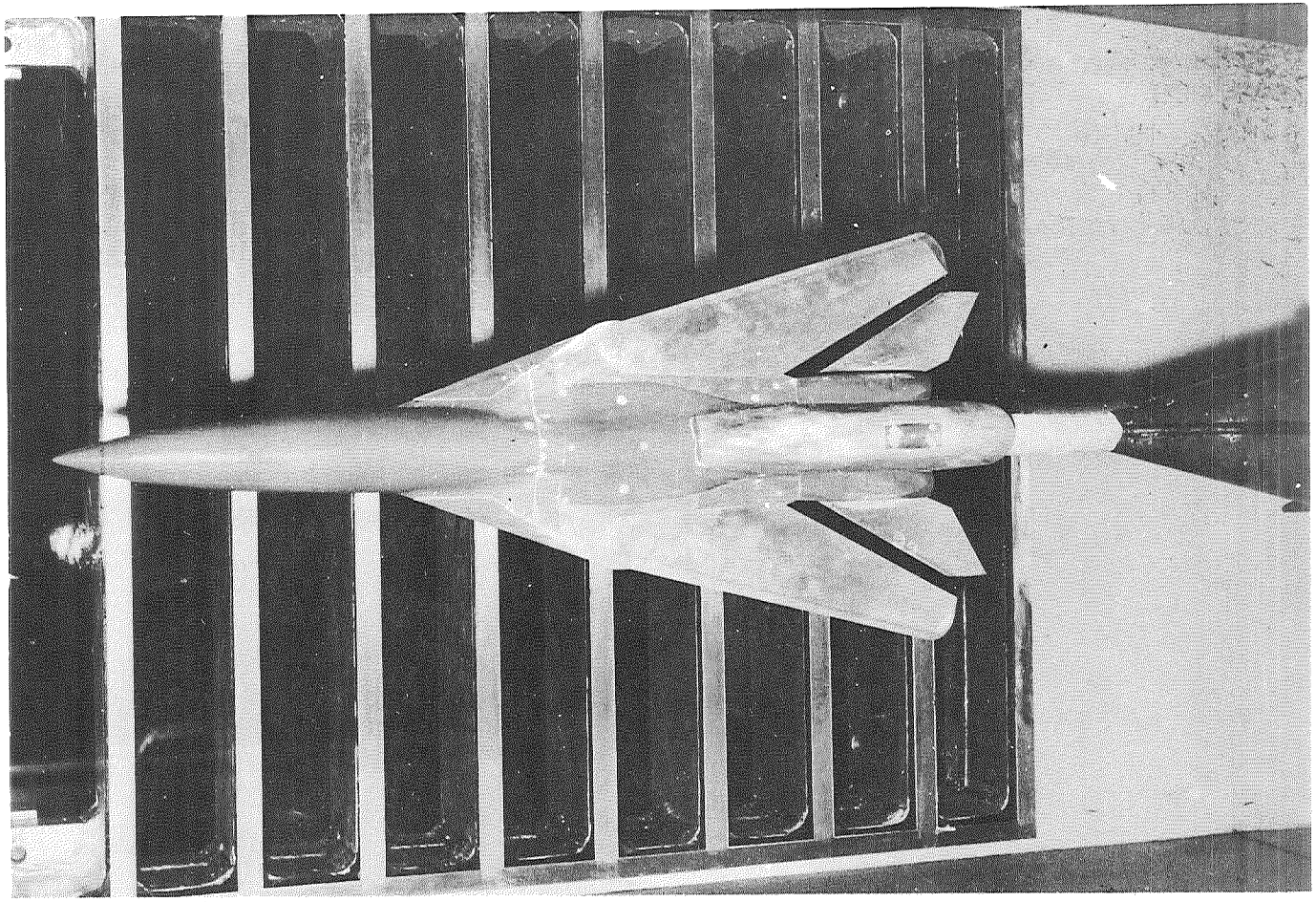

L-70-8036

Figure 6.- Configuration $F_0W_{75}H_1$ installed in test section of Langley Unitary Plan wind tunnel.

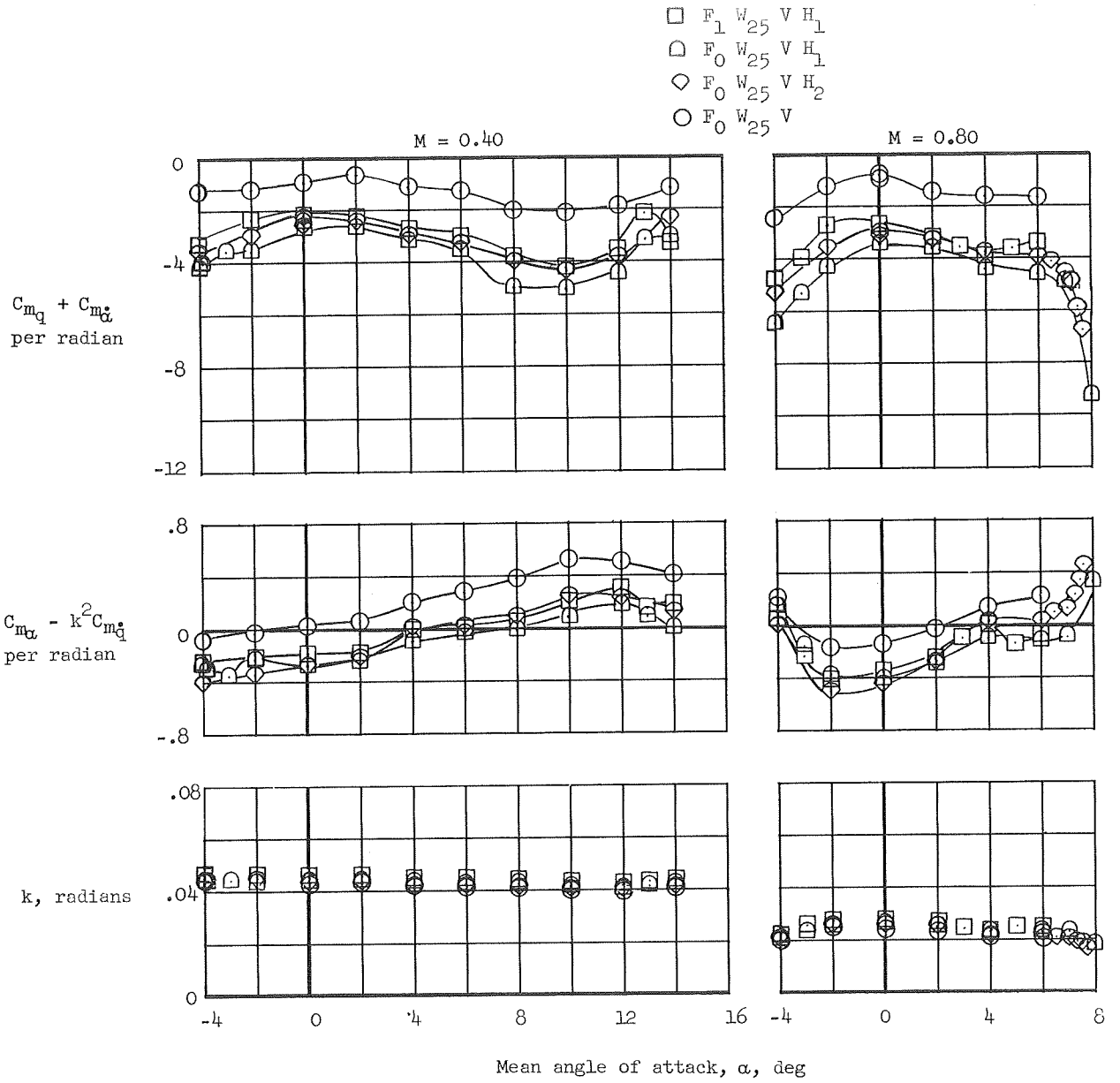

Figure 7.- Variation of longitudinal dynamic stability characteristics with mean angle of attack for sweep of 25°.

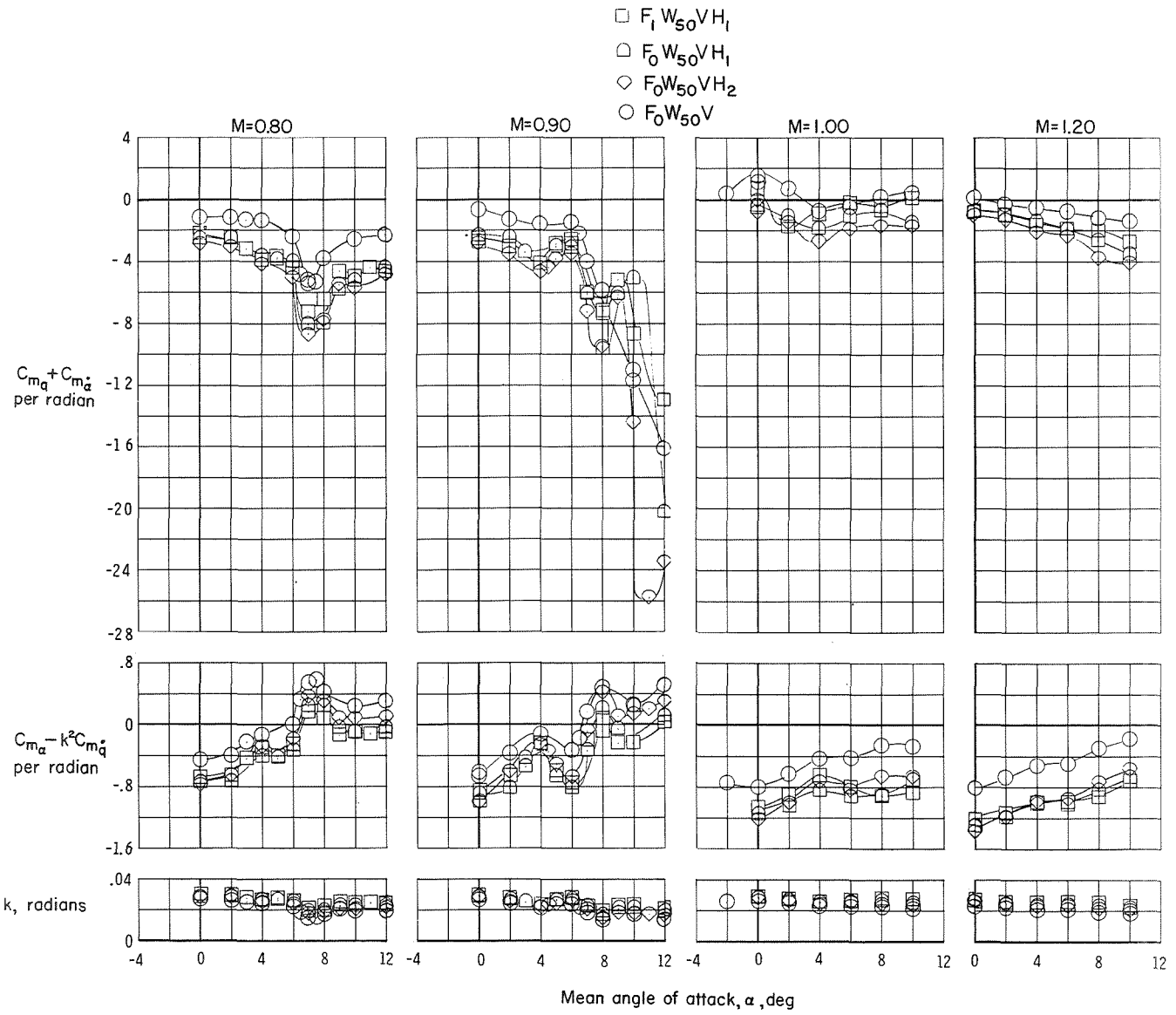

Figure 8.- Variation of longitudinal dynamic stability characteristics with mean angle of attack for wing sweep of 50°.

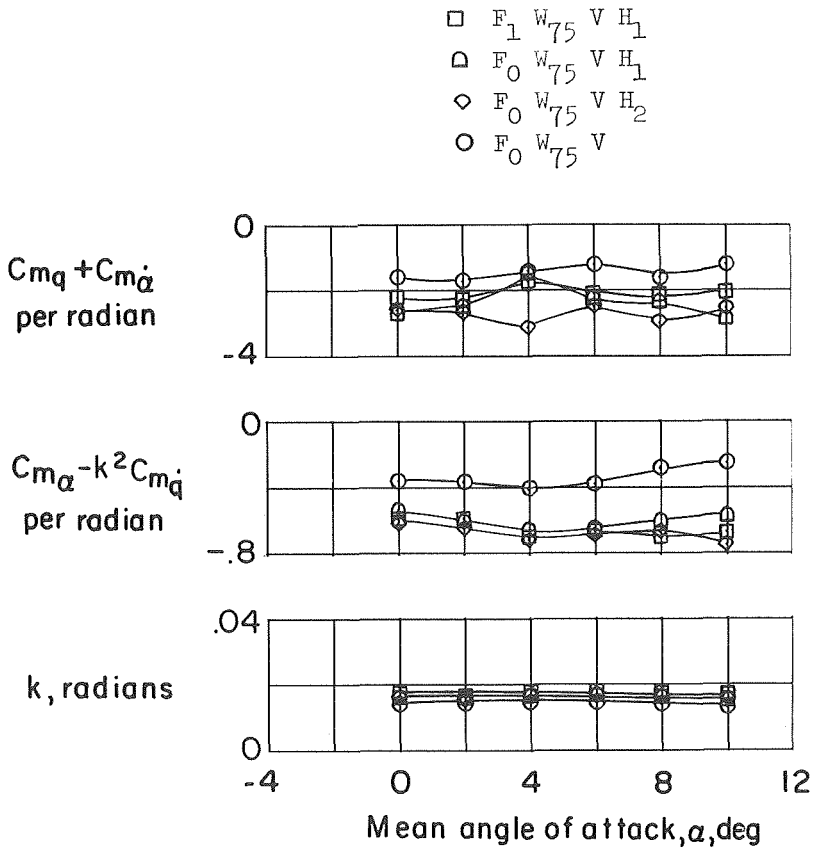

Figure 9.- Variation of longitudinal dynamic stability characteristics with mean angle of attack for wing sweep of 75^{o}. M = 1.80; R = 1.17×10^{6}.

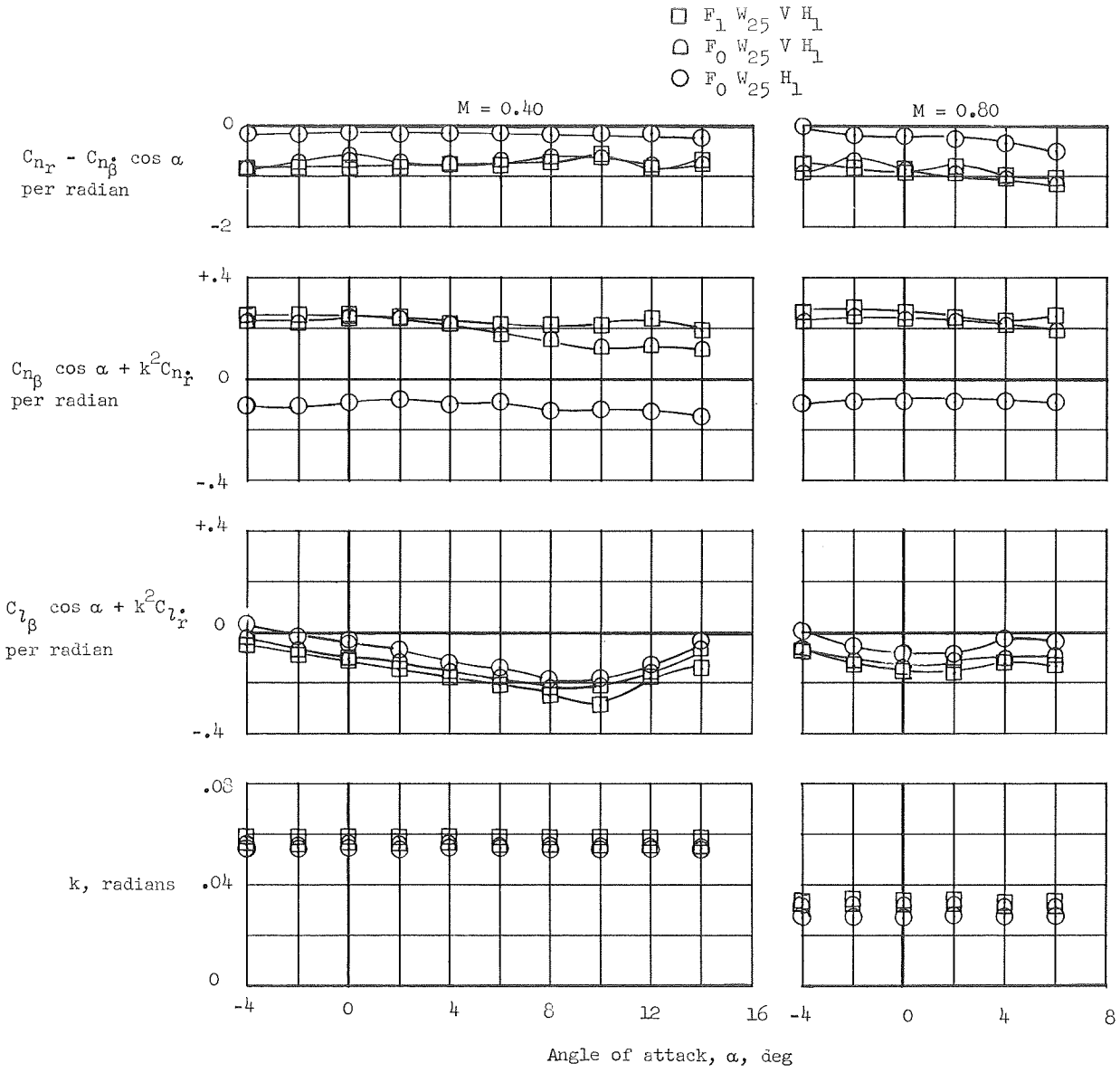

Figure 10.- Variation of lateral dynamic stability characteristics with angle of attack for wing sweep of 25°.

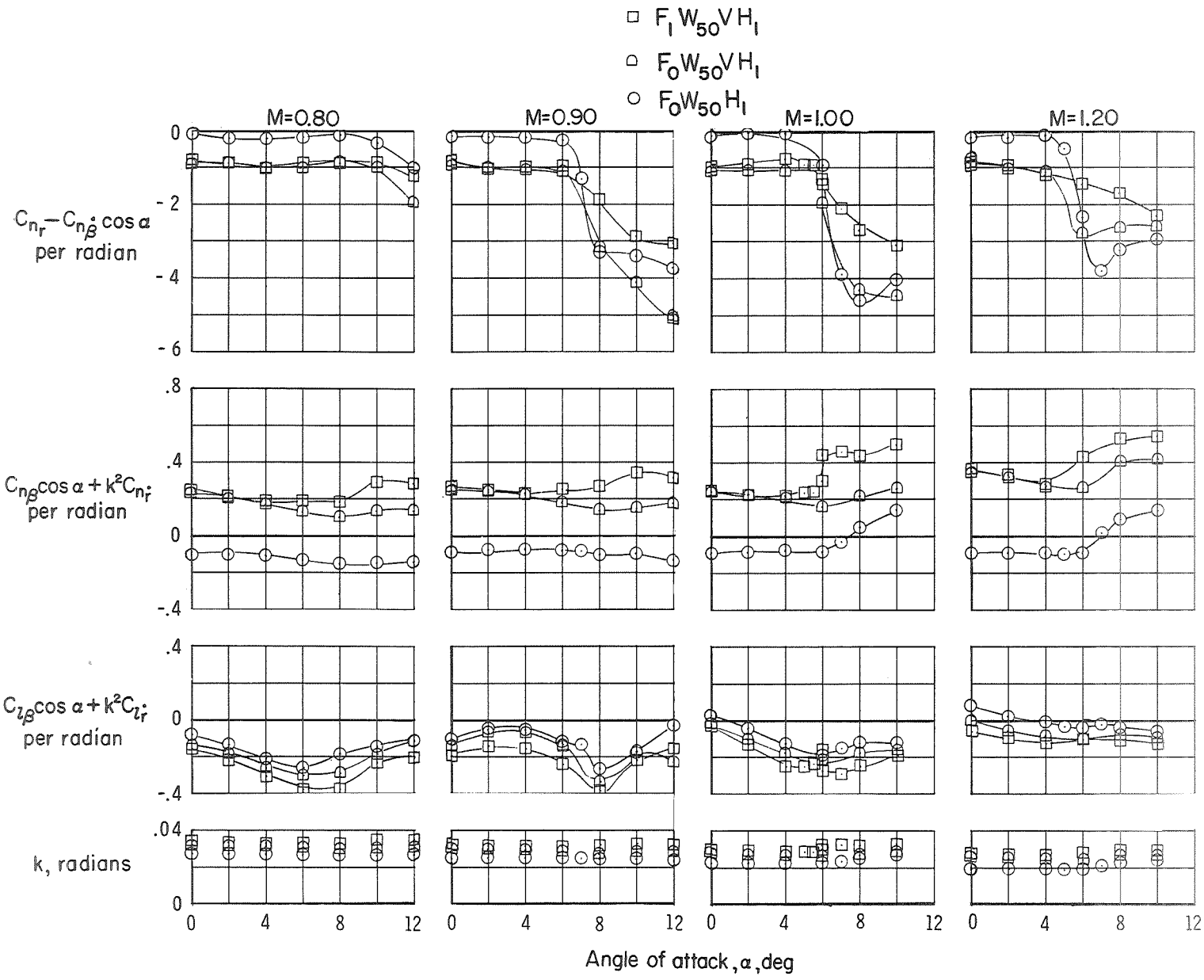

Figure 11.- Variation of lateral dynamic stability characteristics with angle of attack for wing sweep of 50°.

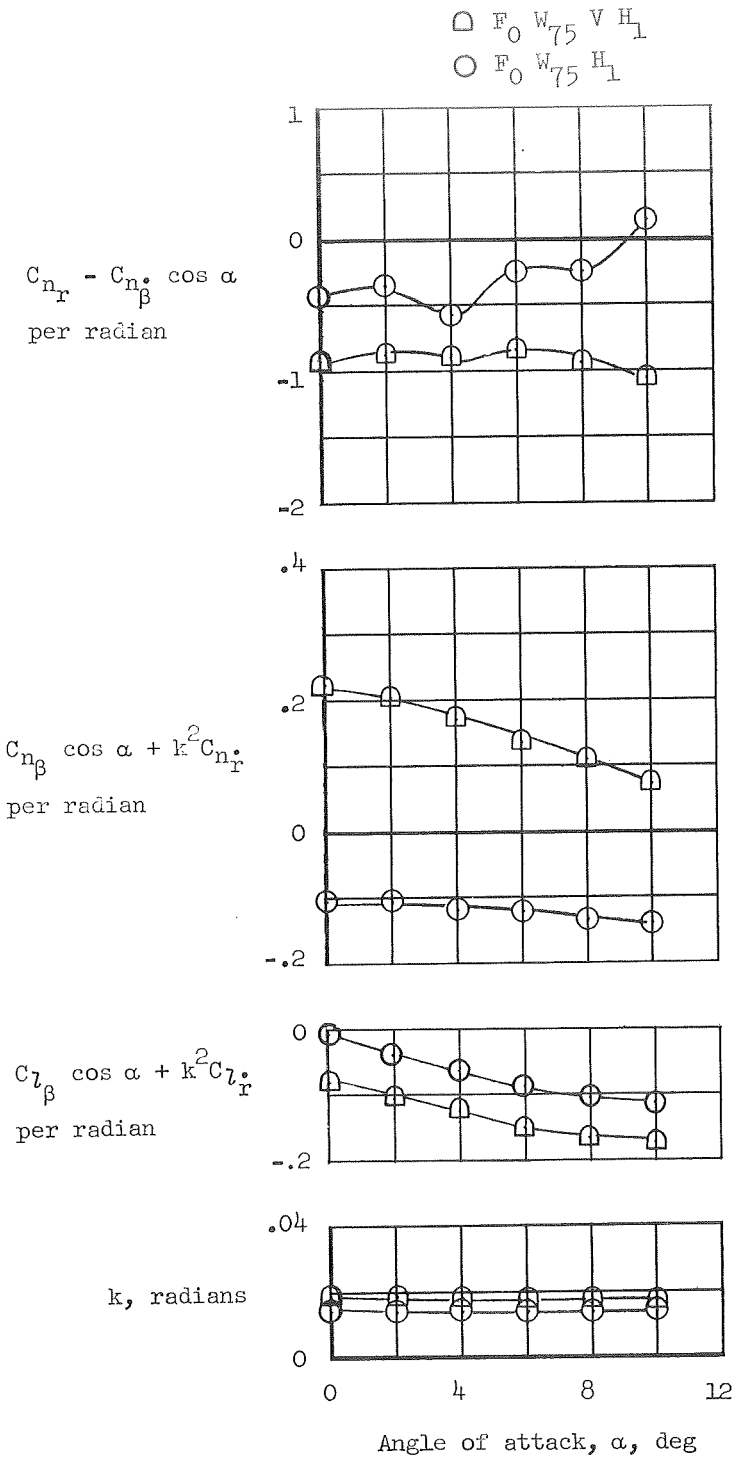

Figure 12.- Variation of lateral dynamic stability characteristics with angle of attack for wing sweep of 75^o. M = 1.80; R = 1.17×10^6.

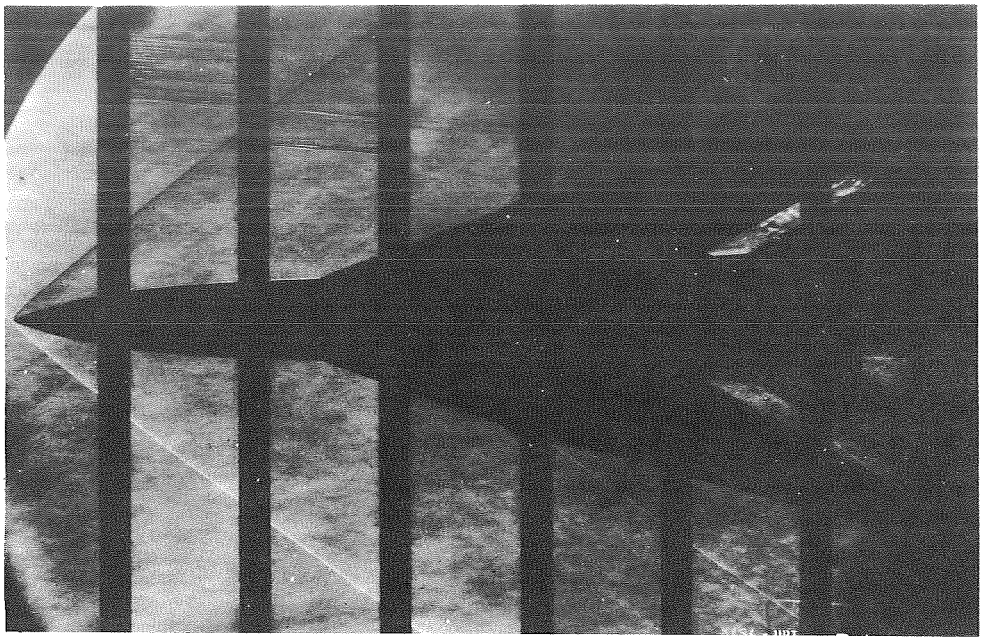

$F_0 W_{75} VH_1$

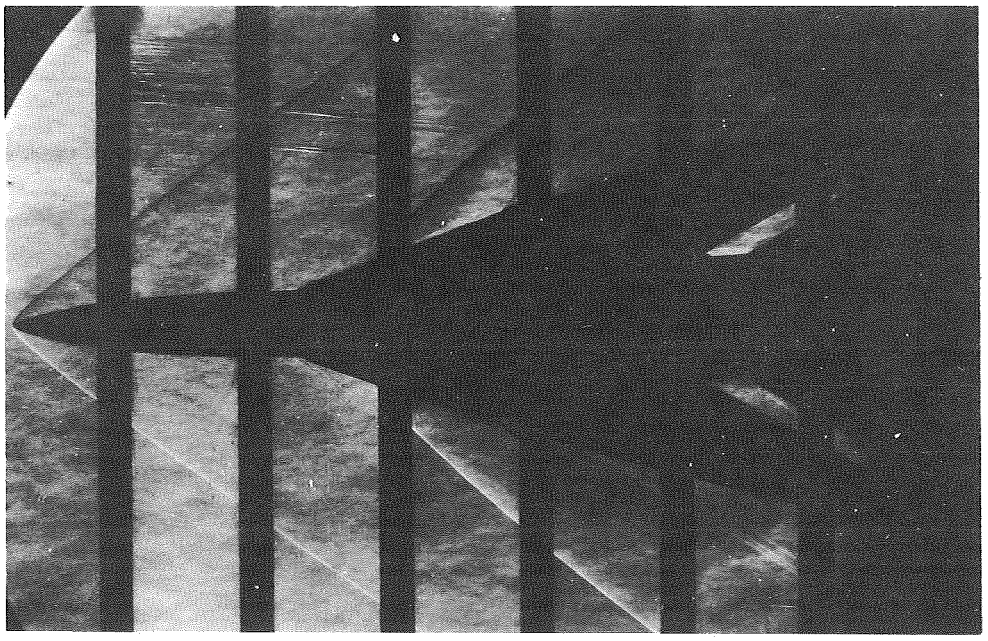

$F_1 W_{75} VH_1$

L-70-8037

Figure 13.- Schlieren photographs obtained at $M = 1.80$ with $\alpha = 0^{\circ}$.

NATIONAL AERONAUTICS AND SPACE ADMINISTRATION
WASHINGTON, D. C. 20546

OFFICIAL BUSINESS

FIRST CLASS MAIL

POSTAGE AND FEES PAID
NATIONAL AERONAUTICS AND
SPACE ADMINISTRATION

POSTMASTER: If Undeliverable (Section 158 Postal Manual) Do Not Return

"The aeronautical and space activities of the United States shall be conducted so as to contribute . . . to the expansion of human knowledge of phenomena in the atmosphere and space. The Administration shall provide for the widest practicable and appropriate dissemination of information concerning its activities and the results thereof."

—NATIONAL AERONAUTICS AND SPACE ACT OF 1958

NASA SCIENTIFIC AND TECHNICAL PUBLICATIONS

TECHNICAL REPORTS: Scientific and technical information considered important, complete, and a lasting contribution to existing knowledge.

TECHNICAL NOTES: Information less broad in scope but nevertheless of importance as a contribution to existing knowledge.

TECHNICAL MEMORANDUMS: Information receiving limited distribution because of preliminary data, security classification, or other reasons.

CONTRACTOR REPORTS: Scientific and technical information generated under a NASA contract or grant and considered an important contribution to existing knowledge.

TECHNICAL TRANSLATIONS: Information published in a foreign language considered to merit NASA distribution in English.

SPECIAL PUBLICATIONS: Information derived from or of value to NASA activities. Publications include conference proceedings, monographs, data compilations, handbooks, sourcebooks, and special bibliographies.

TECHNOLOGY UTILIZATION PUBLICATIONS: Information on technology used by NASA that may be of particular interest in commercial and other non-aerospace applications. Publications include Tech Briefs, Technology Utilization Reports and Technology Surveys.

Details on the availability of these publications may be obtained from:

SCIENTIFIC AND TECHNICAL INFORMATION OFFICE

NATIONAL AERONAUTICS AND SPACE ADMINISTRATION

Washington, D.C. 20546